J Mater Sci (2012) 47:804–814
DOI 10.1007/s10853-011-5858-0

Kinetics of dissolution-precipitation reaction at the surface of small particles: modelling and application

Massimo Tomellini

Received: 30 May 2011 / Accepted: 6 August 2011 / Published online: 24 August 2011

Abstract In the framework of the theory of phase transformations with position-dependent nucleation rate, a model has been developed aimed at describing the dissolution-precipitation reaction at the surface of small particles. The precipitation reaction takes place by nucleation and growth processes under time-dependent supersaturation. Depending on the coverage of the particle surface by the new phase, the reaction kinetics exhibits high- and low-rate regimes. The computation is performed for both progressive and simultaneous nucleation. In the case of simultaneous nucleation, closed-form solutions are attained for diffusion- and interface-limited growth modes and for isotropic and anisotropic growths of the nuclei, as well. The scaling properties of the kinetics on particle size are also investigated. The kinetic model is employed for analysing experimental data and makes it possible to estimate the nucleation density on the particle surface and to have an insight into the microscopic growth law of nuclei.

Introduction

Phase transformations in the solid state are of considerable importance in Materials Science since these phenomena usually occur during the production cycle of materials and affect the microstructure of the final product [1]. With the advent of the nanotechnology, phase transitions, taking place at the surface of small particles, have been attracting considerable interest from both theoretical and experimental points of view. Several studies have been done dealing with phase transitions in one-component systems, which can be schematized as the occurrence of a single reaction. Significant advancements on the modelling of the process have been achieved, which include, among others, the study of the effect on the kinetics of the nucleation rate, of the anisotropic grain growth where the shielding effect comes into play and of the non-random distribution of nuclei as well [2–9]. Numerical and analytical methods have also been developed aimed at describing the particle size distribution function in nucleation and crystallization processes [10–12]. The situation is more involved in the case of transformations taking place in multicomponent systems, owing to the coupling between the mass transport of the various components, as well as to the possible occurrence of multiple reactions [13–15]. A complex reaction that falls within this category is the dissolution-precipitation reaction, which entails, at least, two kinetic processes one of the two, the precipitation, leads to the formation of a new solid phase. An important system that undergoes this type of transformation is the tricalcium silicate (Ca_3SiO_5 i.e. C_3S) when reacting with water. It is a well-established fact that C_3S hydration proceeds via the dissolution of tricalcium silicate and the precipitation of the CaO_x–SiO_2–H_2O (i.e. CSH) phase [16]. The formation of CSH has been shown to occur by heterogeneous nucleation and growth, which depend upon the lime concentration. Since the nucleation stage is much shorter than the duration of the hydration process, the nucleation can be assumed to be simultaneous, a fact that simplifies the modelling of the kinetics and makes it possible to attain solutions in closed form.

The present contribution is aimed at modelling, analytically, the dissolution-precipitation reaction taking place on the surface of small particles and to discuss an application to the study of a real system. In this context, experimental

M. Tomellini (✉)
Dipartimento di Scienze e Tecnologie Chimiche, Università di Roma Tor Vergata, Via della Ricerca Scientifica, 00133, Rome, Italy
e-mail: tomellini@uniroma2.it

data available from the literature are employed as a "test bench" of the approach here developed. The kinetics of precipitation is described in the framework of the theory of phase transitions—ruled by nucleation and growth—in inhomogeneous systems. Besides, the dissolution reaction is coupled with the precipitation process through the rate equation for the supersaturation of the parent phase.

The model kinetics outlined here provides physical insights into the scaling properties of the volume of the new phase, on both particle radius and rate coefficients for the nucleus growth, either for diffusion- or interface-limited growths and isotropic or anisotropic nuclei as well. The supersaturation of the parent phase and the fractional coverage of the particle surface enter the rate equations, explicitly, and permit us to highlight the role of these quantities on the kinetics of the whole process. In addition, keeping the mathematical complexity of the problem manageable, the analytical results can be useful for analysing experimental kinetics in order to estimate the nucleation density at the particle surface, the growth law and the aspect ratio of the nuclei.

The article is divided as follows. In Sect. 2.1, the kinetic model for the precipitation reaction is presented for the general cases of progressive and simultaneous nucleation, as well as for isotropic and anisotropic growths of the nuclei. Section 2.2 is devoted to the kinetics of dissolution-precipitation and to the analysis of experimental data on CSH formation during C_3S hydration.

Results and discussion

The model

The model is based on the theory of nucleation and growth for position-dependent nucleation rate developed in refs. [17–20]. In particular, the nucleation and growth processes, which are subsequent to the dissolution event, are assumed to take place on the surface of a spherical particle. The radius of the particle is considered to be greater than the mean radius of the nuclei.

In the following, the theory is developed for both continuous (i.e. constant nucleation rate) and simultaneous nucleation processes and in the case of nuclei randomly distributed on the particle surface.

Continuous nucleation and isotropic growth

In the case of continuous nucleation, the nucleation rate on the particle surface is taken to be constant, i.e., $\frac{dN}{dt} = I_0$ where N is the surface density of nuclei. Moreover, according to Ref. [20] in the case of isotropic nucleus growth, the growth rate, υ, is taken as constant. With reference to Fig. 1, in what it follows R designates the particle radius, $R_1 = \upsilon(t - t')$ is the nucleus radius at running time t, where $t' < t$ is the birth time of the nucleus and R_0 is the distance of the generic point P from the particle centre. The probability the generic point is untransformed up to time t is given by the expression

$$P(R_0, t) = e^{-\xi_e(R_0,t)}, \tag{1}$$

where ξ_e, a function of R_0, is the so-called extended volume [21, 22] whose functional form will be derived below.

Since the nucleation occurs on the particle surface, the nuclei that start growing at time t' capable of transforming the generic point P up to t are those who lie on the particle surface contained within the "sphere of influence" of the point P, namely the sphere of radius $R_1(t - t') = \upsilon(t - t')$ centred at P (see also Fig. 1). Since the area of this region is given by $A(t, t') = \pi \frac{R}{R_0}\left[R_1^2(t - t') - (R_0 - R)^2\right]$, the extended surface reads

$$\xi_e(R_0,t) = \begin{cases} I_0\pi \int_0^{t-\frac{|R-R_0|}{\upsilon}} \frac{R}{R_0}\left[R_1^2(t-t') - (R_0-R)^2\right]dt' & |R-R_0| < \upsilon t \\ 0 & |R-R_0| > \upsilon t\,, \end{cases} \tag{2}$$

where I_0 is the nucleation rate per unitary surface. For the sake of simplicity, the dependence on particle radius has

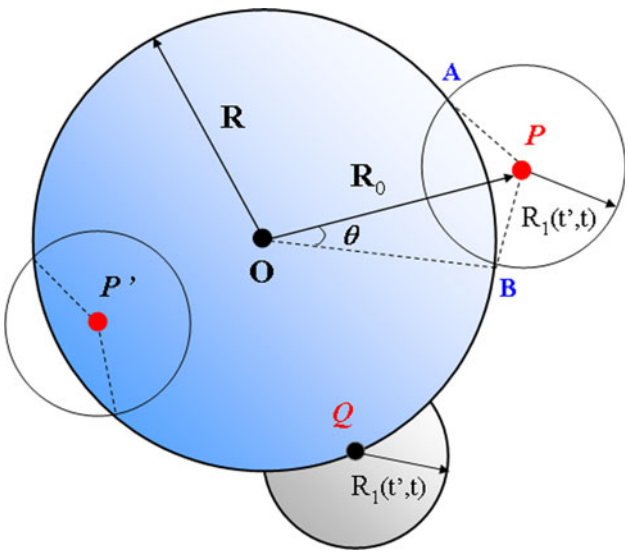

Fig. 1 Representation of the spherical particle, of radius R and of the generic points P and P' above and below the particle surface, respectively. R_1 is the radius of the spherical nucleus nucleated at the particle surface at time t'—at running time t. The sphere of radius R_1 centred at P is the "sphere of influence" of this point. The point P is uncovered by the new phase (i.e. untransformed) provided that no nucleation event occurs (at time t') on the surface of the particle contained within the "sphere of influence", that is, the spherical cup AB. A nucleus centred at Q on the particle surface is also depicted

been omitted in the argument of the ξ_e function. It is worth stressing that this equation holds for transformations involving both the internal ($R > R_0$) and the external portion of the particle. However, with the aim of modelling the precipitation of the new phase from the supersaturated phase, in Eq. 1, the condition $R > R_0$ will be considered, only. For the linear growth law, the integral can be solved leading to the expression

$$\xi_e(\zeta,t) = I_0\pi\upsilon^2 t^3 \frac{\eta}{\zeta}\left\{\frac{2}{3}(\zeta-\eta)^3 + \frac{1}{3} - (\zeta-\eta)^2\right\} \times \Theta[1-(\zeta-\eta)], \tag{3}$$

where $\eta \equiv \eta(t) = \frac{R}{\upsilon t}$, $\zeta \equiv \zeta(t) = \frac{R_0}{\upsilon t}$, $\Theta(x)$ is the Heavyside function ($\Theta(x) = 1$ for $x > 0$; $\Theta(x) = 0$ for $x < 0$) and $\zeta > \eta$. The fraction of untransformed phase is therefore attained by averaging Eq. 1 over the region bounded by the spheres of radii R and $(R + \upsilon t)$:

$$\langle P(t)\rangle = \frac{1}{\frac{4\pi}{3}\left[(R+\upsilon t)^3 - R^3\right]} 4\pi \int_R^{R+\upsilon t} R_0^2 e^{-\xi_e(R_0,t)} \mathrm{d}R_0 = \frac{3}{\left[(\eta+1)^3 - \eta^3\right]} \int_\eta^{1+\eta} \zeta^2 e^{-\xi_e(\zeta,t)} \mathrm{d}\zeta. \tag{4}$$

From Eq. 4, the volume of the transformed phase is computed as

$$V(t) = \frac{4}{3}\pi\left[(R+\upsilon t)^3 - R^3\right](1 - \langle P(t)\rangle). \tag{5}$$

Moreover, by inserting Eq. 3 in Eq. 4, one obtains

$$\langle P(t)\rangle = \frac{3}{\left[(1+\eta)^3 - \eta^3\right]} \int_0^1 (z+\eta)^2 e^{-\frac{Kt^3}{3}\frac{\eta}{z+\eta}\left[1-3z^2+2z^3\right]} \mathrm{d}z, \tag{6}$$

where $z = \zeta - \eta$ and $K = \pi I_0 \upsilon^2$.

It is enlightening to compare Eq. 5 with the solution previously attained by Cahn [23] for nucleated reactions at grain boundaries. This solution, in turn, has also been employed in refs. [24, 25] for modelling dissolution-precipitation processes. In fact, in the limit of planar surface $\eta \to \infty$, and Eqs. 5–6 give

$$V(t) = A\upsilon t\left(1 - \int_0^1 e^{-\frac{Kt^3}{3}(1-3z^2+2z^3)} \mathrm{d}z\right), \tag{7}$$

where A is the area of the surface. On the basis of the argument presented in Ref. [23], in order to deal with an assembly containing a large number of grain boundaries, the volume given by Eq. 5 is considered as the extended volume due to the growth on a single plane. In fact, Eq. 7 gives the contribution of an isolated plane where interference (impingement) between different planes is not allowed. By denoting with V_0 the total volume of the system and with N the total number of planes (grain boundaries), the fraction NV/V_0 plays the role of an extended volume fraction, for multiple overlaps between transformed regions on different planes are now permitted. This extended volume can be related to the volume fraction of the transformed phase, provided that the planes are randomly distributed throughout V_0. A straightforward application of Eq. 1 eventually gives

$$V_T = 1 - e^{-2\frac{NV}{V_0}} = 1 - e^{-2\rho_B\upsilon t\left(1 - \int_0^1 e^{-\frac{Kt^3}{3}(1-3z^2+2z^3)} \mathrm{d}z\right)}, \tag{8}$$

which coincides with the solution of Ref. [23], where $\rho_B = NA/V_0$ is the boundary area per unitary volume. Since the transformation at a grain boundary usually takes place on both sides of the plane, a factor of two has been included in Eq. 8.

As far as the validity of Eq. 8 is concerned, it should be borne in mind that this equation is an approximation. In fact, the statistical argument employed in its derivation and discussed above is not rigorous. The reason for this relies on the so-called blocking effect, which is active whenever the nucleus growth is anisotropic and both distribution and orientation of the nuclei are random [4–7]. Under these circumstances, the Kolmogorov–Johnson–Mehl–Avrami (KJMA) theory [21, 26–29] does not hold. It turns out that, on statistical ground, Eq. 8 is an application of the KJMA theory to phase transitions ruled by simultaneous nucleation and anisotropic growth, where the new phase, nucleated on a single plane, plays the role of the "anisotropic nucleus" (randomly oriented).

Simultaneous nucleation

In the case of simultaneous nucleation, all nuclei start growing at the same time, and the nucleation rate per unitary surface is given by $\frac{\mathrm{d}N}{\mathrm{d}t} = N_0\delta(t)$, where N_0 is the number density of nuclei and $\delta(t)$ is Dirac's delta function. It is worth pointing out that, under these circumstances, the kinetic model can be developed, analytically, for a generic growth law, $R_1 \equiv R_1(t)$. The extended volume fraction reads

$$\xi_e(R_0,t) = N_0\pi\frac{R}{R_0}\left[R_1(t)^2 - (R_0-R)^2\right]\Theta[R_1(t) - (R_0-R)], \tag{9}$$

with $R_0 > R$. Following the computation pathway of the previous section, the mean value of the untransformed fraction (Eq. 6) is given by

$$\langle P(t)\rangle = \frac{3}{\left[(1+\eta)^3-\eta^3\right]}\int_0^1 (z+\eta)^2 e^{-\pi N_0 R_1(t)^2 \frac{\eta}{z+\eta}\left[1-z^2\right]}\mathrm{d}z, \tag{10}$$

with $\eta \equiv \eta(t) = \frac{R}{R_1(t)}$, $\zeta \equiv \zeta(t) = \frac{R_0}{R_1(t)}$ and $z = \zeta - \eta$.

The volume of the new phase is computed using Eq. 5 as

$$V(t) = \frac{4\pi}{3}R_1(t)^3 \times \left[(\eta+1)^3-\eta^3-3\int_0^1 (\eta+z)^2 e^{-\pi N_0 R_1(t)^2 \frac{\eta}{z+\eta}(1-z^2)}\mathrm{d}z\right], \tag{11}$$

where $\zeta_e(z,t) = \pi N_0 R_1(t)^2 \frac{\eta}{z+\eta}(1-z^2)$. In the early stage of the growth, $N_0 R_1^2(t) \ll 1$ and a series expansion of the exponential function entering Eq. 11 provides $V \cong \frac{4\pi R_1^3}{3}\frac{M_0}{2}$, where $M_0 = 4\pi R^2 N_0$ is the total number of nuclei. This is the expected result in the case of non-overlapping nuclei.

With the aim of modelling the dissolution-precipitation reaction, it is convenient to express the kinetics in terms of the fraction of the particle surface that is covered by the precipitate, S. Since an isolated nucleus of radius $R_1(t)$ covers a portion of the particle surface of area $a = \pi R_1^2$, the transformed surface fraction is

$$S(t) = 1 - e^{-y(t)}, \tag{12}$$

where $y = \pi N_0 R_1^2$ is the extended surface. The extended volume of Eq. 11 can eventually be expressed in terms of the quantity S as follows

$$\xi_e(z,S) = \frac{M_0}{4}\frac{(1-z^2)}{(z+\eta)\eta}, \tag{13a}$$

where

$$\eta(S,M_0) = \frac{1}{2}\left(\frac{M_0}{-\ln(1-S)}\right)^{1/2} \tag{13b}$$

and M_0 is the total number of nucleation centres on the particle surface. Besides, the volume of the precipitate can be recast in the form

$$V(y) = \frac{4\pi}{3}R_1(y)^3\left[1+3\left(\frac{M_0}{4y}\right)^{1/2}+3\left(\frac{M_0}{4y}\right) - 3\left(\frac{M_0}{4y}\right)\int_0^1\left(1+\frac{z}{\eta}\right)^2 e^{-\frac{y\eta}{\eta+z}(1-z^2)}\mathrm{d}z\right]. \tag{13c}$$

In the limit $R \gg R_1$ (that is $\eta \gg 1$ or $M_0 \gg y$), the integral in Eq. 13c is independent of M_0 and the transformed volume becomes

$$V(y) = \frac{M_0}{N_0^{3/2}}G(y) \tag{14}$$

where $G(y) = \sqrt{y/\pi}[1-I(y)]$ and $I(y) = \int_0^1 e^{-y(1-z^2)}\mathrm{d}z$.

In view of the application of the kinetics to describe experimental data (Sect. 2.2), before concluding this section, we will briefly discuss the case of anisotropic nucleus growth. Under these circumstances, a simple approach has been developed by assuming the growth rates, normal and tangential to the particle surface, to be different to each other. It is worth pointing out that, since nucleation takes place on the particle surface, in this case, the aforementioned blocking effect is not present. The extended surface (Eq. 9) is

$$\xi_e(R_0,t) = 2\pi N_0 R^2\left(1-\cos\frac{\ell_{//}(t)}{R}\right)\Theta[\ell_\perp(t)-(R_0-R)], \tag{15a}$$

where $\ell_{//}(t)$ and $\ell_\perp(t)$ are, respectively, the growth laws tangential and normal to the particle surface and $R_0 > R$. The probability $\langle P(t)\rangle$ is now given by

$$\langle P(t)\rangle = \frac{3}{\left[(1+\lambda)^3-\lambda^3\right]}e^{-2\pi N_0 R^2\left[1-\cos\frac{\ell_{//}}{R}\right]}\int_0^1 (z+\lambda)^2\mathrm{d}z = e^{-2\pi N_0 R^2\left[1-\cos\frac{\ell_{//}}{R}\right]}, \tag{15b}$$

where $\lambda = \frac{R}{\ell_\perp}$ and $z = (R_0-R)/\ell_\perp$. It is noteworthy that in this case, the fraction of the particle surface covered by nuclei is equal to $S(t) = 1 - \langle P(t)\rangle$. The computation of the transformed volume is performed by exploiting the same approximation that led to Eq. 14, namely the particle size is thought to be greater than the nucleus size. By Taylor expanding the trigonometric function in Eq. 15b, one ends up with

$$V(t) = \frac{4\pi}{3}\ell_\perp^3(t)\left\{(1+\lambda)^3-\lambda^3\right\}\left(1-e^{-\pi N_0 \ell_{//}^2(t)}\right). \tag{16}$$

By defining $y = \pi N_0 \ell_{//}^2(t)$ and retaining in the first bracket the leading term in λ, one obtains

$$V(y) = \frac{\alpha M_0}{N_0^{3/2}}\tilde{G}(y), \tag{17}$$

where $\alpha = \frac{\ell_\perp}{\ell_{//}}$ is the aspect ratio of the nucleus and $\tilde{G}(y) = \sqrt{y/\pi}[1-e^{-y}]$. It is worth emphasizing the similarity between Eqs. 17 and 14, which only differ in the definition of the $I(y)$ function.

The trends of $G(y)$ $\tilde{G}(y)$ are displayed in Fig. 2. For nucleus size which scales as $R_1 \approx \sqrt{t}$ (i.e. $y \approx t$), the G function mimics the kinetics of the transformed volume on

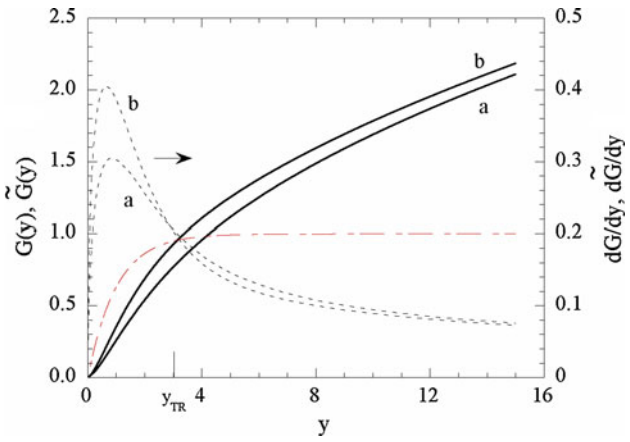

Fig. 2 Behaviour of the $G(y)$ (curve *a*) and $\tilde{G}(y)$ (curve *b*) functions for the isotropic and anisotropic growth modes, respectively. The derivatives of these functions are also displayed as *dashed lines* (*right scale*). The surface coverage is shown as *dashed-dotted line* (*left scale*), and the y value at the transition point, y_{TR}, has been marked on the abscissa

a single particle. Similar consideration holds for $\tilde{G}$, provided that the aspect ratio is constant. The trends of the derivatives of $G(y)$ and $\tilde{G}(y)$ underline the presence of high-rate and low-rate regimes, where the transition- to the low-rate regime occurs once the fractional coverage of the particle surface is nearly one.

Although the simultaneous nucleation has to be considered a model case, it allows us to deal with any growth law and, moreover, to obtain an analytical solution suitable for treating experimental data. In fact, the present approach is suitable for studying the CSH growth on C_3S grains where the nucleation process has been shown to be nearly simultaneous [30]. Besides, in the early stage of the reaction, the effect of the particle radius reduction, owing to the dissolution process, can be faced by properly re-scaling the nucleation rate as $\frac{dN}{dt} \rightarrow \frac{dN}{dt}\left[\frac{R(0)}{R(t)}\right]^2$, where $R(t)$ is the particle radius at running time t. In the case of simultaneous nucleation, the re-scaling simply applies to the nucleation density.

Rate equation for the dissolution-precipitation reaction

This section is devoted to describe the formation, via a dissolution-precipitation process, of a new phase (denoted in this section as the α phase) on a small particle (denoted as the π phase). In view of the application discussed in the last section, the parent phase is considered to be a liquid phase (denoted as the β phase) and the supersaturation (undersaturation) of a single species is assumed to rule the reaction.

The kinetics of the transformed volume (Eqs. 5, 11) has to be coupled with the kinetics of growth of the nuclei, which, in turn, is expected to be an involved function of the transformed volume. In fact, such a close coupling between nucleus growth law and phase transition kinetics is due to the fact that the dissolution process depends upon the fraction of the particle surface covered by the precipitate, S. Accordingly, the changing rate of the supersaturation of the parent phase is due to both "interface-controlled" and "diffusion-limited" (within the precipitate) reactions of π and β phases. The first contribution is proportional to $(1 - S)$, while the second, being ruled by Fick's law, is proportional to the ratio $S/\bar{h}$, where $\bar{h} = \frac{V}{4\pi R^2 S}$ is the mean thickness of the precipitate. In the following, to simplify the complexity of the mathematical computation, we thought the growth as ruled by the supersaturation of one component, referred to as the active species. Accordingly, for isotropic growth of the nuclei, the rate equations for the dissolution and the growth of the α phase read,

$$\left(\frac{dn}{dt}\right)_{diss} = 4\pi R^2\left[k_1\frac{S}{\bar{h}} + k_2(1-S)\right] \tag{18a}$$

$$\left(\frac{dn}{dt}\right)_{prec} = c_\alpha\frac{dV}{dt} = c_\alpha\frac{M_0}{N_0^{3/2}}\frac{dG}{dt}, \tag{18b}$$

where n is the number of active species in the parent phase, c_α is the concentration of active species in the precipitate and the k_is are the rate coefficients. It is useful to switch from the n variable to the supersaturation of the active species in the parent phase (with respect to the α phase) that is defined as [31, 32] $\sigma \equiv \sigma_{\beta,\alpha} = \frac{c-c_\beta}{c_\alpha - c_\beta}$, with c_β being the concentration of the active species in the solution in equilibrium with the precipitate. Since the rate equation for the supersaturation in a system of constant volume, say v_0, is $\frac{d\sigma}{dt} = \frac{1}{(c_\alpha - c_\beta)v_0}\frac{dn}{dt}$, Eqs. 18a,b lead to the balance equation,

$$\begin{aligned}\frac{d\sigma}{dt} &= \frac{1}{\Delta c v_0}\left[\left(\frac{dn}{dt}\right)_{diss} - \left(\frac{dn}{dt}\right)_{prec}\right] \\ &= \bar{k}_2\left\{S\left(\tilde{k}_1\frac{S}{G} - 1\right) + 1\right\} - k_3\frac{dG}{dt},\end{aligned} \tag{19}$$

where $\bar{k}_2 = \frac{4\pi R^2 k_2}{\Delta c v_0}$, $\tilde{k}_1 = \frac{k_1}{k_2}N_0^{1/2}$, $k_3 = \frac{c_\alpha M_0}{\Delta c N_0^{3/2} v_0}$ and the short notation $\Delta c = c_\alpha - c_\beta$ was used. In the following, the reasonable assumption is made according to which $c_\alpha \gg c_\beta$, i.e., $\Delta c \cong c_\alpha$. The rate constants for dissolution are proportional to the supersaturation of the π phase with respect to the β phase, namely $\sigma \equiv \sigma_{\pi,\beta} = \frac{c'_\beta - c}{c'_\beta - c_\pi}$, where c'_β is the concentration of the species in the solution in equilibrium with the phase π. In fact, the β phase is supersaturated (undersaturated) with respect to the α (π) phase. It turns out that for $c'_\beta \gg c$, the rate coefficients for dissolution are independent of c. Eqs. 18, 19 also apply to the case of anisotropic nucleus growth by substituting G

with $\alpha\tilde{G}$, that is, using Eq. 17 in place of Eq. 14. Moreover, Eq. 19 can be rewritten in terms of the variable $y = \pi N_0 R_1^2$, provided that the growth law is known. For instance, in the case of diffusion-limited growth [33] $\frac{dR_1}{dt} = D\frac{\sigma}{R_1}$ and $\frac{dy}{dt} = 2\pi N_0 D\sigma$, D being the diffusion coefficient of the active species in the parent phase. On the other hand, in the case of interface-limited growth, the rate is independent of R_1 and one obtains, $\frac{dy}{dt} \propto \sqrt{y}\sigma$ (see also the Appendix). For diffusion-limited growth, Eq. 19 eventually becomes

$$\frac{d\sigma^2}{dy} = A\left\{S\left(\tilde{k}_1\frac{S}{G} - 1\right) + 1\right\} - B\frac{dG}{dy}\sigma, \tag{20}$$

where $A = \frac{\bar{k}_2}{\pi N_0 D}$, $B = 2k_3$ and the functions $S(y)$, $G(y)$ are given by Eqs. 12, 14. Once Eq. 20 has been solved for $\sigma(y)$, the $y(t)$ function can be estimated through integration of the growth rate according to

$$\tau = \int \frac{dy}{\sigma(y)}, \tag{21}$$

where $\tau = 2\pi N_0 Dt$ is the dimensionless time. The time dependence of the volume of the α phase, grown on a single particle, is eventually obtained through Eq. 14 and the $y(\tau)$ function Eq. 21. It goes without saying that under steady-state conditions, Eq. 20 is identically nil, σ is constant and the reaction rate is just given by the time derivative of Eq. 14 (or Eq. 17). This computation, however, requires the knowledge of the $y(t)$ function. In turn, this function can be determined either through modelling or from experimental data.

We are now in a position for determining the scaling properties of the parameters A, B and $\tilde{k}_1$ in Eq. 20. To this end, let us consider the reaction of N_p spherical particles, equal in size, with the liquid parent phase at constant temperature. Accordingly, the volume of solution that pertains to a single particle is, on average, $v_0 \cong \frac{\Omega}{N_p} = \frac{\Omega\rho_\pi 4\pi R^3}{3m}$ where Ω is the volume of the solution, N_p the number of particles, m the total mass of the particles and ρ_π the density of the π phase. As discussed in the last section, in the nucleation stage, the total number of nuclei can be considered to depend only on the initial mass of the π phase. Consequently, one gets $\frac{m}{\rho_\pi 4\pi R^3/3}4\pi R^2 N_0 = \text{const.}$ that is $N_0 = wR$, w being a constant. For the coefficients A, B and $\tilde{k}_1$ entering Eq. 20, one obtains the following scaling relationships with particle radius:

$$A = \frac{3mk_2}{c_\alpha \pi w D\rho_\pi \Omega}\frac{1}{R^2} \tag{22a}$$

$$B = \frac{6m}{\Omega w^{1/2}\rho_\pi}\frac{1}{R^{3/2}} \tag{22b}$$

$$\tilde{k}_1 = \frac{k_1}{k_2}w^{1/2}R^{1/2}, \tag{22c}$$

where the total volume of the precipitate is given by

$$V_T(\tau) = N_p V(\tau) = \frac{3m}{\rho_\pi w^{1/2}}\frac{1}{R^{3/2}}G(y(\tau)). \tag{22d}$$

It is worth pointing out that the function $G(\tau)$ also depends on R via N_0. Furthermore, as reported in the Appendix, Eq. 20 can be solved in closed form provided that the supersaturation does not change, substantially, during the reaction. The integration of Eq. 20 is performed by considering the initial value of the supersaturation, σ_0, different from zero. The reason for this is that nucleation has been assumed to be simultaneous, i.e., at the beginning of the phase transformation, the nucleation process is already completed. Since nucleation and growth require a supersaturation value different from zero, we set $\sigma \neq 0$ at $t = 0$.

The kinetics of the transformed volume, for both diffusion- and interface-limited growths of isotropic nuclei, is shown in Fig. 3 (see also the Appendix). In particular, the kinetics of the total volume and supersaturation is displayed in Fig. 3a and c for several values of the particle radius at $\sigma_0 = 0.1$. The dimensionless time has been properly re-scaled to the particle radius, owing to the dependence of N_0 on R. In this plot, the quantities reported in the abscissa and in the ordinate are proportional to the running time and to the volume of the new phase, respectively. The solution of the rate equations (Fig. 3) gives account, qualitatively, of the two kinetic regimes, experimentally observed in the dissolution-precipitation reaction, and characterized by high rate and low rate. The induction time of the dissolution-precipitation reaction is found to be longer for the interface-limited growth mechanism. It should be borne in mind that since these solutions are expressed in terms of dimensionless variables, they are "universal" in the sense that they only depend on growth mode and nucleus shape. The transition to the low-rate regime of the kinetics is ascribed to the slow down of the dissolution process once the fractional surface coverage, S, approaches unity. In fact, this explanation is consistent with the behaviour of the $S(\tau)$ kinetics also shown in Fig. 3b and d. The behaviour of the supersaturation curve, as well as the presence of a maximum, depends on parameter values and growth mechanism. Furthermore, at given values of A, B and A', no appreciable change in the reaction kinetics is obtained for $\tilde{k}_1 < 0.01$, which is therefore representative of the lowest value of the reaction rate, once the particle surface has been entirely covered by the precipitate.

It is worth emphasizing that the precipitation reaction proceeds until the supersaturation becomes nil, since the

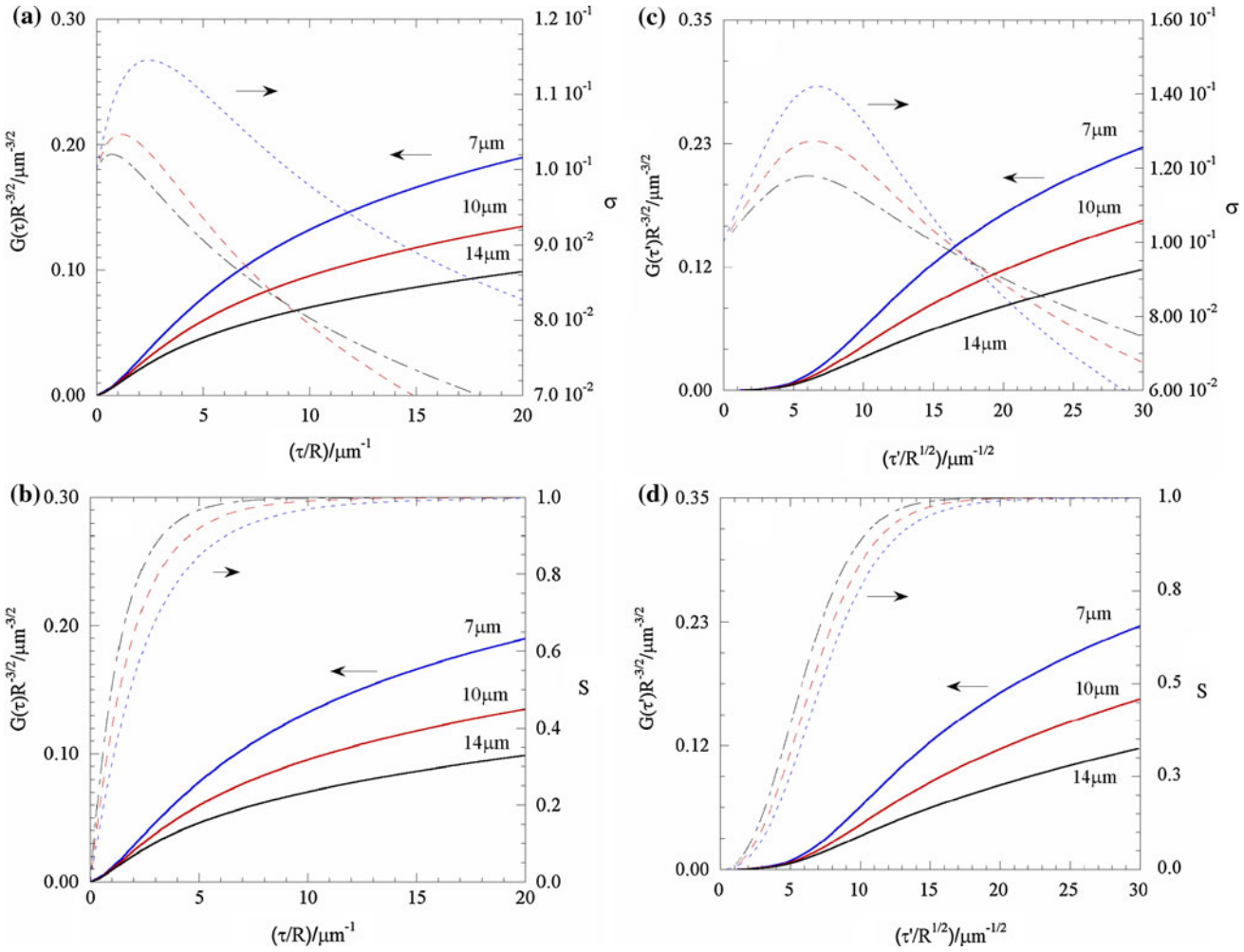

Fig. 3 Solution of the kinetics for isotropic and both diffusion (**a**, **b**) and interface (**c**, **d**)-limited growths of the nuclei (Eqs. 25–26) at $\sigma_0 = 0.1$. The kinetics refers to the reaction on particles of diameters 7, 10 and 14 μm. The behaviour of the supersaturation and fraction of particle surface covered by the precipitate are shown in (**a**, **c**) and (**b**, **d**), respectively (*right scale*). *Dashed lines*: particle diameter 7 μm; *long dashed lines*: particle diameter 10 μm; *dashed-dotted lines*: particle diameter 14 μm. Parameter values for $2R = 7$ μm are $A = A' = 10^{-2}$; $\beta = 0.1$; $\tilde{k}_1 = 0.01$. Values of A, A', B and $\tilde{k}_1$ at the various R satisfy the scaling relationships Eqs. 22, 27

time derivative of the volume of the new phase is proportional to the supersaturation σ. In turn, this time derivative enters the last term of the rate equation Eq. 20.

Application of the model to the formation of CSH layer during C_3S hydration: analysis of the experimental kinetics

The reaction of formation of Calcium Silicate Hydrate (CSH) on anhydrous grains, during Ca_3SiO_5 (C_3S) hydration, is important in Materials Science and Engineering for C_3S and is the main constituent of Portland cement, and the hardening of the material is found to be governed by the hydration process. Specifically, the dissolution and the precipitation reactions are according to $Ca_3SiO_5 + 3H_2O \rightarrow 3Ca^{2+} + 4OH^- + H_2SiO_4^{2-}$ and $xCa^{2+} + 2(x-1)OH^- + H_2SiO_4^{2-} \rightarrow CaO_x - SiO_2 - H_2O$, respectively, where x is the CaO/SiO_2 ratio. Recently, the kinetics of this reaction, together with the effect of nanoparticles of foreign solid phase on the hydration process, has been studied in Refs. [24, 25, 30]. As far as the description of the kinetics is concerned, it is usually done by using either the standard KJMA model or, as recently discussed in Ref. [24], Cahn's theory of grain boundary nucleated reactions. In the following, we employ the model presented in Sect. 2.1 for describing the kinetics of growth of CSH at the surface of C_3S particles, where the nucleation process has been shown to be nearly simultaneous [30]. With reference to the notation employed in Sect. 2.1.3, α and π phases are here identified with the CSH and C_3S phases, respectively.

The hydration has been carried out on samples of C_3S particles with different values of the mean diameters and at constant value of the lime concentration. In fact, maintaining constant the concentration of lime avoids any dependence of the growth rate with the $Ca(OH)_2$ concentration. Different brackets of Ca_3SiO_5, equal in mass, have been hydrated in a thermoregulated cell at constant volume. It was shown that in the nucleation stage, the total number of nuclei can be considered to depend only on the mass of C_3S and lime concentration, and the dissolution-precipitation reaction occurs under steady-state conditions [30]. Under these circumstances, the quantity of CSH precipitated can be computed by exploiting the mass balance of Ca^{2+}. In fact, in order to maintain the lime concentration constant, at steady-state, $(3 - x)$ mol of Ca^{2+} have to be removed from the solution per each mole of CSH precipitated. Therefore, by measuring the quantity of Ca^{2+} ions taken from the solution, it is possible to estimate the quantity of CSH precipitated. As far as the modelling is concerned, the volume of CSH can be estimated through Eqs. 14, 17 provided that both nucleation density and microscopic growth law are known (i.e. the $y(t)$ function).

The trends of the $G(y)$, $\tilde{G}(y)$ and $S(y)$ functions, displayed in Fig. 2, indicate that the onset of the low-rate region can be located at a value of the y variable that is around $y_{TR} \cong 3$. This argument is at the basis of an analysis of the kinetic data, which makes it possible to estimate the nucleation density. In fact, the quantity of material precipitated at the transition point, Q_{TR}, can be linked to the nucleation density through Eqs. 14, 17 (depending on the growth mode). Taking into account the total number of particles, one obtains

$$Q_{TR} = \rho_{CSH} \frac{M_0}{N_0^{3/2}} N_p G(y_{TR}) = \frac{\rho_{CSH}}{\rho_{C_3S}} \frac{3m}{R} \frac{1}{N_0^{1/2}} G(y_{TR}) \quad \text{(isotropic growth)} \qquad (23a)$$

$$Q_{TR} = \rho_{CSH} \frac{\alpha M_0}{N_0^{3/2}} N_p \tilde{G}(y_{TR}) = \frac{\rho_{CSH}}{\rho_{C_3S}} \frac{3m}{R} \frac{\alpha}{N_0^{1/2}} \tilde{G}(y_{TR}) \text{ (anisotropic growth)}, \qquad (23b)$$

where Q_{TR}/mol, ρ_{CSH}/mol cm^{-3}, ρ_{C_3S}/g cm^{-3} and N_0/cm^{-2}. The nucleation densities, computed through Eqs. 23 by using the experimental values of Q_{TR}, have been displayed in Fig. 4 for isotropic and anisotropic growths, respectively. In particular, in the present calculation, the numerical values $m = 4$ g, $\alpha = 3$, $\rho_{CSH} = 2.116$ g cm^{-3}, $\rho_{C_3S} = 3.14$ g cm^{-3} and $x = Ca/Si = 1.8$ were employed. In the early stage of the reaction, the quantity of nucleated CSH is expected to depend on the C_3S quantity and lime concentration only, and the ratio $\frac{N_0}{R}$ should be independent of R. The behaviour of the

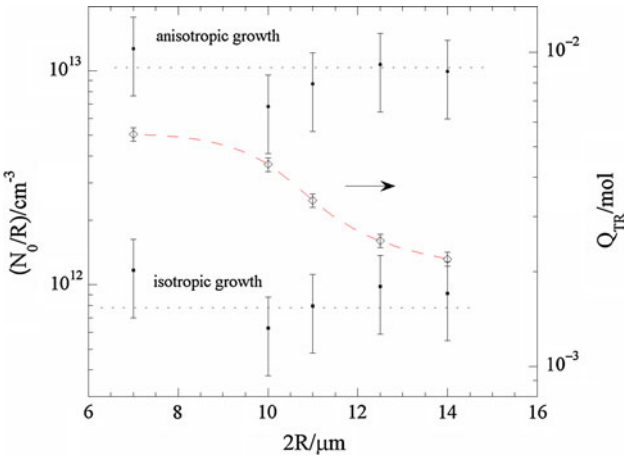

Fig. 4 Behaviour of the re-scaled nucleation density (N_0/R) as a function of particle diameter for both anisotropic (with $\alpha = 3$) and isotropic growths (*left scale*). The computation is performed through Eq. 23 by using the quantities of CSH precipitated at the transition point, Q_{TR} (*right scale*). The *error bar* of N_0/R was estimated from the uncertainties on Q_{TR} and particle radius. Specifically, $\Delta Q_{TR}/Q_{TR} \approx 0.05$ and $\Delta R/R \approx 0.1$ were employed

re-scaled nucleation density has been displayed in Fig. 4. From this figure, it turns out that, assuming an isotropic nucleus growth, the nucleation density is about an order of magnitude lower than that attained in the case of anisotropic growth. In fact, a morphological study of the deposit via AFM corroborates this growth mechanism. Significantly, the values of the nucleation density computed in Fig. 4 for the anisotropic growth are in agreement with those employed in the numerical simulation discussed in Ref. [30]. In this computer simulation, the mole fraction of nuclei (for instance at $2R = 7$ μm) was 4×10^{-5}, which implies, assuming a density of surface sites of the order of magnitude of $\rho_0 \cong (\rho_{C_3S})^{2/3}$, an $N_0 \cong 10^{10}$ cm^{-2}. Therefore, the present data analysis, based on an analytical approach, is consistent with the kinetic results previously achieved on the growth mode of the deposit.

Once the nucleation density has been estimated, Eqs. 14, 17 can be employed for determining, from the experimental kinetics, the microscopic growth law of the nuclei. To this purpose, the experimental kinetics $Q(t)$ (reproduced in Fig. 5a) has been fitted with a *guess* function that meets the following requirements: (i) it can easily be inverted with respect to the time variable, t; (ii) it reproduces both the high-rate and low-rate regions of the experimental kinetics. The low-rate region is nearly linear with time, while the high-rate region is found to be well described by a stretched exponential curve. Furthermore, step functions can suitably be employed for modelling the transition between these two reaction regimes. The function $Q(t) = \omega[1 - \exp(-\gamma t^p)]\Theta(t^* - t) + [q(t - t^*) + Q(t^*)]\ \Theta(t - t^*)$ has therefore been used ($\Theta(x)$ being the

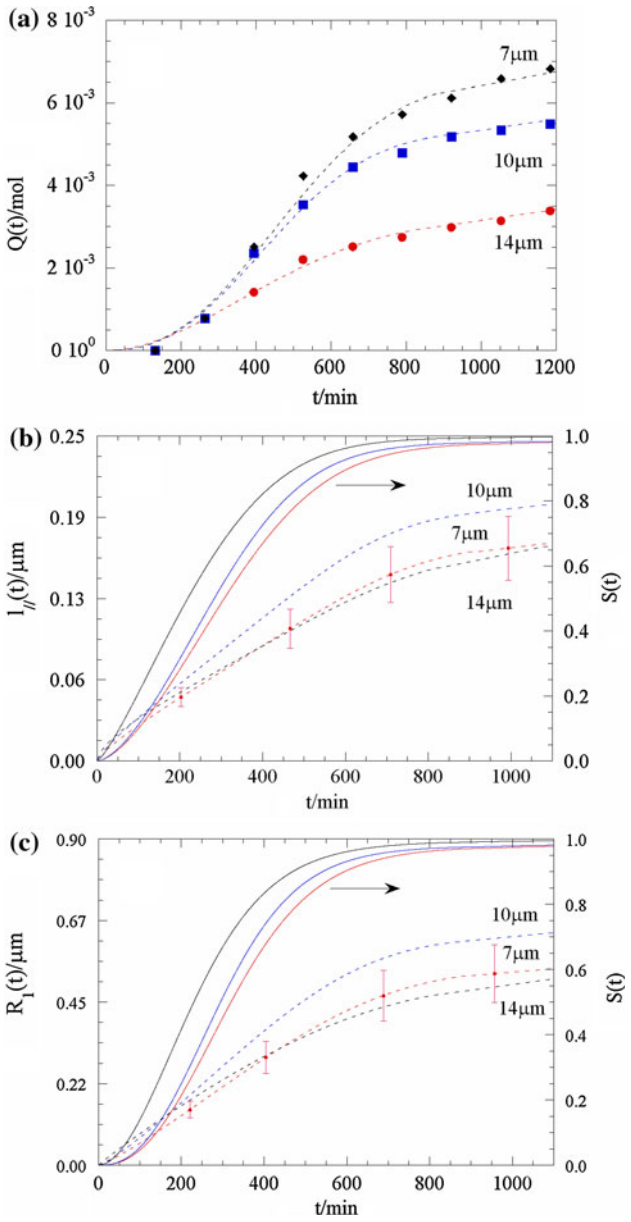

Fig. 5 **a** Experimental data on the kinetics of CSH formation (reproduced from Ref. [30]). The *dashed line* is the best fit of the guess function reported in Sect. 2.2 to the data. **b** and **c** show the behaviour of the microscopic growth law by assuming anisotropic and isotropic growth modes, respectively (*dashed lines*). The behaviour of the fraction of the particle surface covered by the precipitate is also shown (*right scale, solid lines*). The typical *error bar* is also displayed. From the top of the figures **b** and **c**, the $S(t)$ curves refer to 14, 10, and 7μm particle diameters

Heavyside function), where ω, γ and p are fitting parameters and q is the slope of the linear part of the low-rate region of the kinetics. The cut-off time, t^*, has been chosen in such a way as to ensure the continuity of the derivative. The fits are shown in Fig. 5a as dashed lines and provide us with a description of the kinetics through an analytical function. By inverting this function and inserting either the $Q_{\mathrm{th}}(y) = \frac{Q_{\mathrm{TR}}}{G(y_{\mathrm{TR}})} G(y)$ (isotropic growth) or the $Q_{\mathrm{th}}(y) = \frac{Q_{\mathrm{TR}}}{G(y_{\mathrm{TR}})} \tilde{G}(y)$ (anisotropic growth) curves, one gets

$$t(y) = \left[-\frac{1}{\gamma} \ln\left(1 - \frac{Q_{\mathrm{th}}(y)}{\omega}\right) \right]^{1/p} \Theta(Q(t^*) - Q_{\mathrm{th}}(y)) + \left[\frac{Q_{\mathrm{th}}(y) - Q(t^*)}{q} + t^* \right] \Theta(Q_{\mathrm{th}}(y) - Q(t^*)),$$

that is the $y = y(t)$ function. The growth laws, $\ell_{//}(t) = \left(\frac{y(t)}{\pi N_0}\right)^{1/2}$ and $R_1(t) = \left(\frac{y(t)}{\pi N_0}\right)^{1/2}$, are eventually computed for anisotropic and isotropic growths, respectively. It is worth pointing out that it is at the level of the determination of the $y = y(t)$ function, and therefore of the microscopic growth law, that the kinetic model developed in Sect. 2.1.2 comes into play in this analysis with the $G(y)$ ($\tilde{G}(y)$) function. In addition, the microscopic growth law is for the extended size of the nucleus (R_1, $\ell_{//}$) as discussed in Ref. [21, 22]. The results have been shown in Fig. 5b–c for three values of the mean diameter of the particles and for the two nucleus shapes although, as discussed above, the anisotropic case is more appropriate. The uncertainties $\delta R_1/R_1$ and $\delta \ell_{//}/\ell_{//}$ have been considered of the order of magnitude of $\delta N_0/N_0$ which, in turn, depends on both $\delta Q_{TR}/Q_{TR}$ and $\delta R/R$ through Eqs. 23. This kinetics is found to be almost linear with time, at least in the high-rate region. Such a behaviour seems to be compatible with an interface-limited growth under constant value of supersaturation, since this growth mechanism entails $\dot{\ell}_{//} \approx \sigma$. Besides, a nearly constant supersaturation indicates that this stage of the growth proceeds under quasi-steady-state conditions, i.e., the dissolution and precipitation reactions occur at the same rate.

The experimental kinetics indicates that the dissolution-precipitation reaction also proceeds after the duration of the experiment, namely $\approx$ 1200/min, although this rate is about one order of magnitude lower than that of the high-rate region. On the other hand, the rate of growth of the nuclei, as extracted from the data by means of the kinetic model (Fig. 5b–c), is found to be different from zero at the maximum time of the kinetic curve. The quantity of material precipitated on a single particle at the maximum time can be computed from the growth law of Fig 5b according to: $\alpha \ell_{//} 4\pi R^2 \rho_{\mathrm{CSH}}$ and the fraction of C_3S converted to CSH can be computed as: $3\alpha \ell_{//} \rho_{\mathrm{CSH}} / R \rho_{C_3S}$. For instance, on a 14-μm-diameter particle, the percentage of precipitated material is $(20 \pm 5)\%$, at $\alpha = 3$, which favourably compares with a value of 20% as computed from the experimental curve of Fig. 5a; on a 10-μm-diameter particles, this value is $(24 \pm 6)\%$ to be compared with a value of 30% attained from Fig. 5a. In these evaluations, the rate of dissolution is assumed to be equal to the rate of precipitation. The uncertainties of these estimates

are linked to those of particle radius and nucleus size, $\ell_{//}$, as discussed.

Before concluding this section, a comment is in order on the effect of the particle shrinkage caused by the dissolution process in the early stage of the reaction. Since the rate of dissolution is nearly equal to the rate of precipitation, the relation holds

$$R(t) \cong R(0)\left[1 - \frac{3(\mathrm{PM})_{\mathrm{C_3S}}}{4\pi\rho_{\mathrm{C_3S}}N_p R(0)^3}Q(t)\right]^{1/3} = R(0)\left[1 - \frac{(\mathrm{PM})_{\mathrm{C_3S}}}{m}Q(t)\right]^{1/3}, \quad (24)$$

where $(\mathrm{PM})_{\mathrm{C_3S}}$ is the molecular weight. According to Sect. 2.1, an estimate of the nucleation density at the transition point is given by $N_0(R_0)/N_0(R_{\mathrm{TR}}) = \left[1 - \frac{(\mathrm{PM})_{\mathrm{C_3S}}}{m}Q_{\mathrm{TR}}\right]^{2/3}$. This ratio is found to be 0.8, 0.82 and 0.92 for $2R_0 = 7$, 10 and 14 μm, respectively.

Conclusions

In this contribution, it has been shown that the kinetic theory of phase transition with position-dependent nucleation rate can successfully be applied for describing complex transformations, occurring in multicomponent systems, such as the dissolution-precipitation reaction. The reaction kinetics exhibits two regimes characterized by high and low rates. The onset of the second regime is ruled by the kinetics of the surface coverage of the particle. The model is developed for both progressive and simultaneous nucleation. In the last case, the solution is obtained in closed form for any growth law and in terms of dimensionless variables. The model is employed for analysing experimental data on the formation of CSH at C_3S particles, in order to get information on both nucleation density and growth law. By using the quantity of CSH precipitated up to the transition point between the high- and the low-rate regions, the nucleation density has been estimated to be in the range 10^9–10^{11} cm^{-2}, depending on the particle radius. As far as the microscopic growth law is concerned, it was derived from the experimental kinetics and it is consistent with the interface-limited growth mechanism.

Appendix

By setting in Eq. 20 $z = \sigma^2$ and expanding the function $\sqrt{z}$, in the last term of the right member, up to the second order around $z_0 = \sigma_0^2$, one ends up with the equation ($G' = \frac{\mathrm{d}G}{\mathrm{d}y}$)

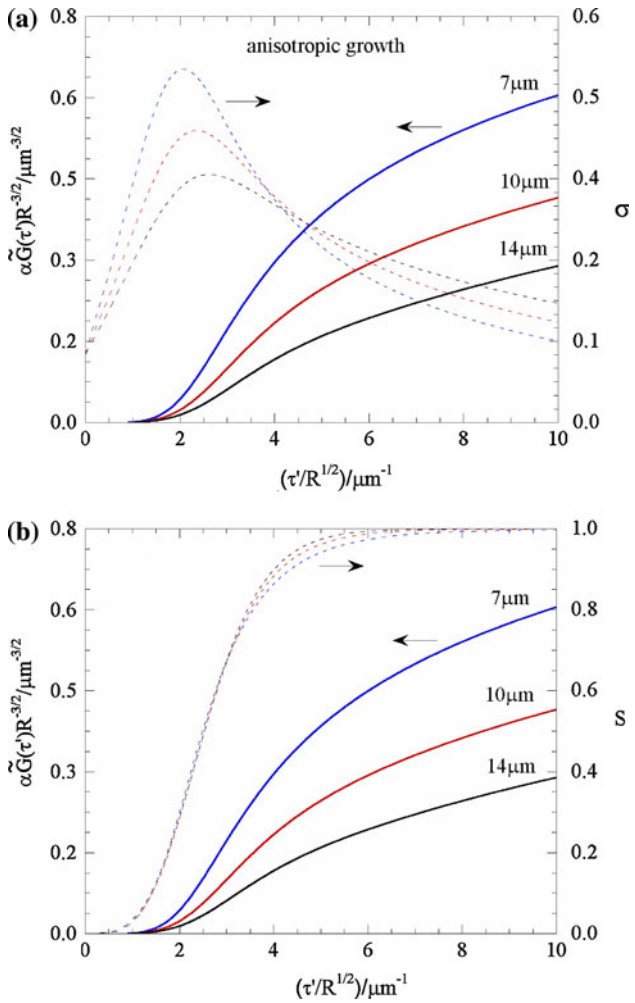

Fig. 6 Kinetics of transformation in the case of interface-limited growth of anisotropic nuclei (*left scale*). The initial supersaturation and the aspect ratio are equal to $\sigma_0 = 0.1$ and $\alpha = 3$, respectively. Values of B and $\tilde{k}_1$ as in Fig. 3. The quantity A' scales as $A'(2R) \approx R^{-3/2}$ where $A'(7\,\mu m) = 0.3$. The supersaturation and the fractional surface coverage of the particles are shown as *dashed lines* in **a** and **b**, respectively (*right scale*). The maximum of the supersaturation decreases with particle radius, and the changing rate of the fractional surface coverage increases with particle radius

$$\frac{\mathrm{d}z}{\mathrm{d}y} + z\frac{\beta}{\sigma_0}G'(y) = f(y) \quad (25)$$

with solution

$$z(y) = e^{-\frac{\beta G(y)}{\sigma_0}}\left(\sigma_0^2 + \int_0^y f(x)e^{\frac{\beta G(x)}{\sigma_0}}\mathrm{d}x\right), \quad (26)$$

where $\beta = \frac{3}{4}B$, σ_0 is the initial supersaturation and $f(y) = A\left\{S(y)\left(\tilde{k}_1\frac{S(y)}{G(y)} - 1\right) + 1\right\} - \frac{\beta\sigma_0}{2}G'(y)$. In Eq. 25, the terms of the order of z^2 have been neglected. As anticipated above, using Eq. 26 in Eq. 21, one estimates $y(\tau)$ and, with it, the time dependence of the volume of the

new phase. In turn, in Fig. 3, the behaviour of the supersaturation is consistent with the series expansion above, since $\sigma^2 \ll 1$. The reaction kinetics exhibits a transition from high-rate to low-rate regimes, which is ruled by the surface coverage of the particle (Fig. 3).

In the case of interface-limited growth of isotropic nuclei, the growth rate is proportional to the supersaturation ($\dot{R}_1 = b\sigma$) and $\frac{dy}{dt} = 2b\sigma\sqrt{\pi N_0 y}$ where b is a constant. Eq. 20 becomes

$$\frac{d\sigma^2}{dy} = \frac{A'}{\sqrt{y}}\left\{S\left(\tilde{k}_1\frac{S}{G} - 1\right) + 1\right\} - B\sigma\frac{dG}{dy}, \qquad (27)$$

where $A' = \frac{\bar{k}_2}{b\sqrt{\pi N_0}} = \frac{3k_2 m}{b\Delta c\sqrt{\pi w}\rho_{C_3S}\Omega R^{3/2}}$, to be compared with Eq. 22a. Therefore, provided that the series expansion of $\sqrt{z}$ holds in this case as well, the approximate solution of Eq. 27 is still given by Eq. 26 with A replaced by $\frac{A'}{\sqrt{y}}$. The dimensionless time is now given by $\tau' = \int \frac{dy}{\sqrt{yz(y)}}$ (see also Eq. 21) where $\tau' = 2b\sqrt{\pi N_0}t$.

By using in Eq. 27, the function $\alpha\tilde{G}(y)$ instead of $G(y)$, this equation can also be employed for modelling the anisotropic nucleus growth. Solutions of Eq. 27, in the case of interface-limited growth of anisotropic nuclei, are displayed in Fig. 6a–b. Even in this case, the kinetics exhibits the presence of high- and low-rate regions and of an induction time.

References

1. Schmalzried H (1974) Solid state reactions. Academic Press, Inc, New York, London
2. Weinberg MC, Zanotto ED (1989) J Non-Cryst Solids 108:99
3. Shneidman VA, Weinberg MC (1993) J Non-Cryst Solids 160:89
4. Birnie DP, Weinberg MC (1995) J Chem Phys 103:3742
5. Kooi BJ (2004) Phys Rev B 70:14110
6. Pusztai T, Gránásy L (1998) Phys Rev B 57:14110
7. Song SJ, Liu F, Jiang YH, Wang HF (2011) Acta Mater 59:3276
8. Fanfoni M, Tomellini M, Volpe M (2002) Phys Rev B 65:172301
9. Rios PR, Oliveira JCPT, Oliveira VT, Castro JA (2006) Mater Res 9:165
10. Farjas J, Roura P (2007) Phys Rev B 75:184112
11. Farjas J, Roura P (2008) Phys Rev B 78:144101
12. Teran AV, Bill A, Bergmann RB (2010) Phys Rev B 81:075319
13. Starink MJ (2004) Int Mater Rev 49:191
14. Liu F, Sommer F, Bos C, Mittemeijer EJ (2007) Int Mater Rev 52:193
15. Yu G, Lee ST, Lai JK (1998) Phys Rev B 57:13573
16. Fierens P, Verhaegen JP (1976) Cement Concrete Res 6:337
17. Weinberg MC (1992) J Non-Cryst Solids 142:126
18. Alekseechkin NV (2001) J Phys Condens Matter 13:3083
19. Alekseechkin NV (2008) Condens Matter Phys 11:597
20. Tomellini M (2010) J Mater Sci 45:733. doi:10.1007/s10853-009-3992-8
21. Kolmogorov AN (1937) URSS Bull Acad Sci URSS (Cl Sci Math Nat) 3:355
22. Shepilov MP, Baik DS (1994) J Non-Cryst Solids 171:141
23. Cahn JW (1956) Acta Metall 4:449
24. Thomas JJ (2007) J Am Ceram Soc 90:3282
25. Lee BY, Kurtis KE (2010) J Am Ceram Soc 93:3399
26. Avrami M (1939) J Chem Phys 7:1103
27. Avrami M (1940) J Chem Phys 8:212
28. Avrami M (1941) J Chem Phys 9:177
29. Johnson WA, Mehl RF (1939) Trans Am Inst Min Metall Pet Eng 135:416
30. Garrault S, Behr T, Nonat A (2006) J Phys Chem B 110:270
31. Tomellini M (2003) J All Comp 348:189
32. Tomellini M (2008) J Mater Sci 43:7102. doi:10.1007/s10853-008-3024-0
33. Zener C (1949) J Appl Phys 20:950